

ARTICLE OPEN

Giant power factors in p- and n-type large-area graphene films on a flexible plastic substrate

Kaito Kanahashi¹, Masatou Ishihara², Masataka Hasegawa², Hiromichi Ohta³ and Taishi Takenobu^{1,4*}

This study reports on the thermoelectric properties of large-area graphene films grown by chemical vapor deposition (CVD) methods. Using the electric double layer gating technique, both the continuous doping of hole or electron carriers and modulation of the Fermi energy are achieved, leading to wide-range control of the Seebeck coefficient and electrical conductivity. Consequently, the maximum power factors of the CVD-grown large-area graphene films are 6.93 and 3.29 mW m⁻¹ K⁻² for p- and n-type carrier doping, respectively. These results are the best values among large-scale flexible materials, such as organic conducting polymers and carbon nanotubes, suggesting that CVD-grown large-area graphene films have potential for thermoelectric applications.

npj 2D Materials and Applications (2019)3:44; <https://doi.org/10.1038/s41699-019-0128-0>

INTRODUCTION

Recently, the rapid development of wearable electronics and sensors has led to the concept of the “Internet of Things” (IoT).^{1,2} In this idea, a network of billions of smart devices that connect people, systems and other applications collect and share data, providing key information for artificial intelligence (AI) as well as realizing a smart society. However, most wearable devices are still powered by batteries that are subject to frequent recharging and replacement. Therefore, this powering problem is one of the serious limiting factors for a future IoT society. One possible solution for wearable devices without a battery is energy harvesting technologies, and among them, thermoelectric energy conversion based on flexible materials has attracted much attention over the years.^{1,2} To date, flexible large-scale thermoelectric conversion devices have been investigated in van der Waals materials, such as organic conducting polymers, carbon nanotubes (CNTs) and their composites,^{3–11} and the best power factors among them are 2.71 and 2.46 mW m⁻¹ K⁻² for p-type and n-type devices, respectively.^{7,11}

Another promising van der Waals material is graphene. In micron-scale single-crystal graphene films, extremely high maximum power factors of 36.0 and 19.0 mW m⁻¹ K⁻² have already been reported in p-type and n-type devices, respectively, although micron-scale single crystals are too small to apply in wearable devices.^{12–14} Moreover, centimeter-scale polycrystalline graphene films have been produced by chemical vapor deposition (CVD), opening a pathway for the development of flexible large-scale thermoelectric conversion devices.^{15,16} Therefore, we can conclude that a CVD-grown large-area graphene film is one of the potential candidates for the power generator for IoT devices. However, to the best of our knowledge, there is no report on the thermoelectric properties of large-area graphene films on a flexible substrate.

Here, we investigated the thermoelectric properties of CVD-grown polycrystalline graphene films on plastic substrates. To perform p- and n-type doping, we fabricated electric double layer transistors (EDLTs) of graphene films.^{17,18} By combining

thermoelectric measurements and the EDLT technique, we continuously controlled the Seebeck coefficient and electrical conductivity. We observed maximum power factors of 6.93 and 3.29 mW m⁻¹ K⁻² for p- and n-type carrier doping, respectively, which exceeds the best previously reported results.

RESULTS

Thermoelectric properties of CVD-grown large-area graphene films

We used CVD-grown large-area graphene films on a polyethylene terephthalate (PET) substrate.¹⁶ The details of the synthetic procedure are provided in Experimental section. The average layer number and grain size of the resultant graphene films are estimated to be two (see Supplementary Information S1) and ~10 nm, respectively.^{19–21} Figure 1a shows a schematic illustration of device fabrication. The original centimeter-scale graphene film on the PET substrate was cut into smaller pieces. Then, to pattern the graphene film, we used an adhesive tape as a shadow mask and removed excess graphene film by an O₂ plasma treatment. Afterwards, Au/Ni electrodes were thermally deposited onto the graphene samples, forming the four-point-probe configuration. Importantly, we introduced a long channel length of 0.4 mm and a channel width of 2 mm to introduce a clear temperature difference between the source and drain electrodes for reliable thermoelectric measurements. For the gate dielectric layer, we prepared an ion gel film, which is a mixture of an ionic liquid, *N,N*-diethyl-*N*-(2-methoxyethyl)-*N*-methylammonium bis-(trifluoromethylsulfonyl)-imide ([DEME][TFSI]), and an organic polymer, poly(vinylidene fluoride-co-hexafluoropropylene) (P(VDF-HFP)).

Figure 1b shows the current-voltage curves using the four-point-probe configuration in the graphene-based EDLT on the PET substrate. We used a semiconductor parameter analyzer (Agilent Technologies, Inc. B1505A) and nanovoltmeter (Keysight, 34420 A) to collect the data, and all measurements were performed in an N₂-filled glove box at room temperature. We applied drain voltages ranging from -0.1 to 0.1 V and simultaneously

¹Department of Advanced Science and Engineering, Waseda University, Tokyo 169-8555, Japan. ²Nanomaterials Research Institute, National Institute of Advanced Industrial Science and Technology (AIST), Ibaraki 305-8565, Japan. ³Research Institute for Electronic Science, Hokkaido University, Sapporo 001-0020, Japan. ⁴Department of Applied Physics, Nagoya University, Nagoya 464-8603, Japan. *email: takenobu@nagoya-u.jp

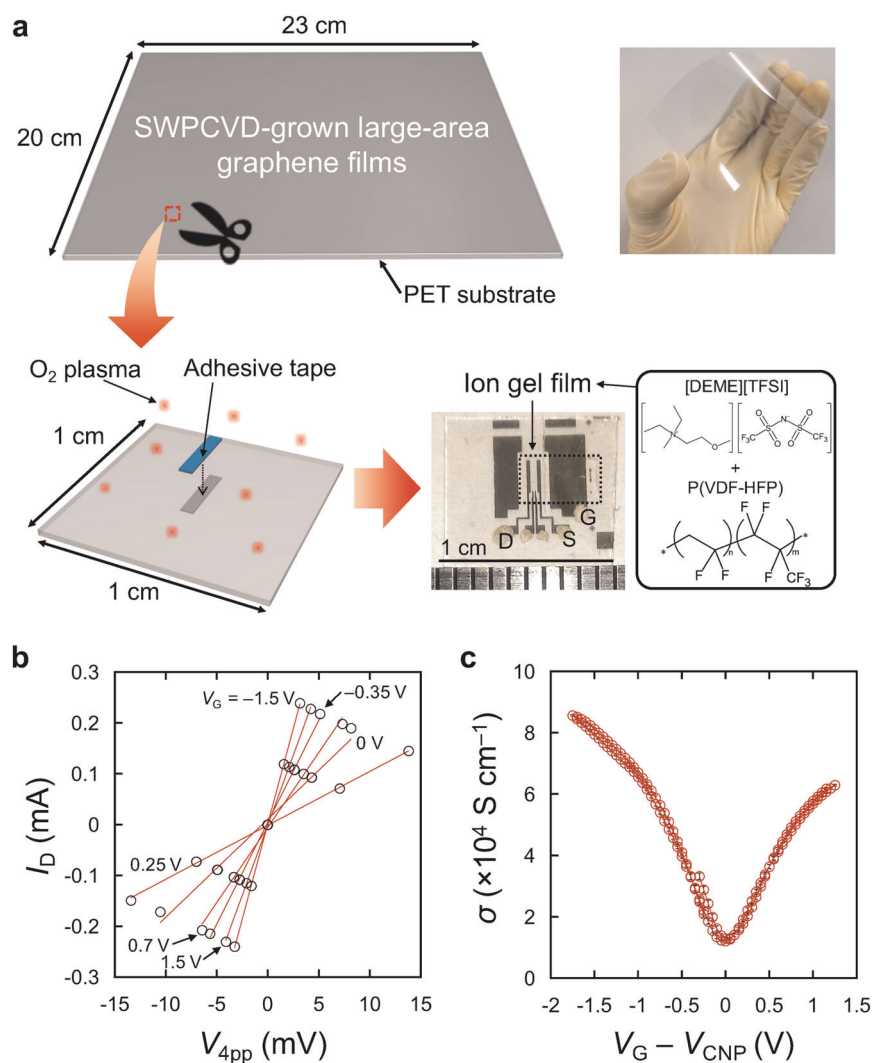


Fig. 1 **a** Schematic illustration of a procedure for fabricating an EDLT sample using CVD-grown large-area graphene films on a PET substrate. An optical image of the graphene-based EDLT sample with the four-point-probe configuration is also indicated. The ion gel film is a mixture of an ionic liquid, [DEME][TFSI], and an organic polymer, P(VDF-HFP). The scale bar corresponds to 1 cm. **b** The drain current (I_D) – voltage (V_{4pp}) curves at various gate voltages. A drain voltage ranging from -0.1 to 0.1 V was applied. **c** The four-point-probe electrical conductivity (σ) as a function of $V_G - V_{CNP}$

monitored both the drain current (I_D) and the voltage drop (V_{4pp}) at each gate voltage. During the measurement, the gate leakage current was less than 5 nA, indicating that the electrochemical reduction and/or oxidation of ions at the interface of the graphene film was negligible. The four-point-probe electrical conductivity was estimated by linear fitting of the $I_D - V_{4pp}$ curves and thickness of the graphene bilayer (0.7 nm), which was approximated from the Raman spectra results (see Supplementary Information S1). The average standard error of the four-point-probe electrical conductivity is 571 S cm^{-1} , which is smaller than 6% of each fitting result. Additionally, Fig. 1c shows the gate voltage dependence of the four-point-probe electrical conductivity. The minimum electrical conductivity indicates the charge neutrality point (CNP), in which the hole carrier density and electron carrier density are equal. Therefore, in Fig. 1c, we represent the applied gate voltage, V_G , in the relative gate voltage from V_{CNP} (i.e., $V_G - V_{CNP}$). As shown in Fig. 1c, ambipolar characteristics are clearly observed, suggesting the carrier doping of holes and electrons into the graphene films by the formation of electric double layers (EDLs).

Along with the measurements of the $I_D - V_{4pp}$ curves, we also investigated the V_G dependence of the Seebeck coefficient (S) in

the graphene-based EDLT using the method established for transition metal dichalcogenide (TMDC) monolayers.²² A schematic illustration of the thermoelectric measurement system is shown in Fig. 2a.^{22–25} The measurement details are provided in the Experimental section. As shown in Fig. 2a, two thermocouples were directly placed onto the surface of the graphene-based EDLT sample, and the temperature difference ($\Delta T = T_A - T_B$) was induced by two Peltier elements. Both the ΔT and generated thermoelectromotive force (ΔV) were simultaneously measured. The S was calculated as the slope of the $\Delta V - \Delta T$ profiles based on the definition of $S = \Delta V / \Delta T$. At a fixed gate voltage, we continuously measured the four-point-probe electrical conductivity and the Seebeck coefficient. Next, we repeated these measurements at various gate voltages.

Figure 2b represents the $\Delta V - \Delta T$ profiles, in which we obtained linear $\Delta V - \Delta T$ responses for all measurements. In particular, the average standard error in all linear fitting results is $0.28 \mu\text{V K}^{-1}$, indicating that the derived S from our results is reliable. Because the sign of S depends on the type of majority carriers, both positive and negative S values should be observed in the ambipolar EDLTs for p- and n-type transistor operations, respectively.^{22,24,25} Figure 2c shows the $V_G - V_{CNP}$ dependences

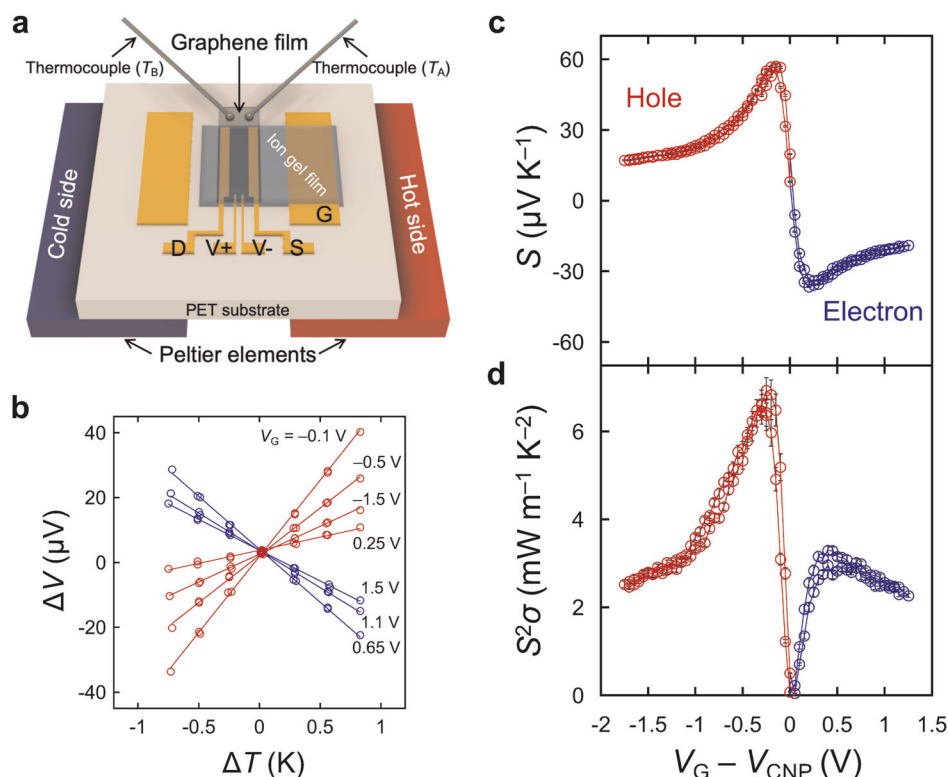


Fig. 2 **a** A schematic of the experimental setup for the thermopower measurements. The right-side temperature (T_A) and the left-side temperature (T_B) are measured by K-type (alumel–chromel) thermocouples. **b** The $\Delta V - \Delta T$ profiles measured at various gate voltages. The red and blue colors indicate the hole and electron carriers, respectively. **c** The Seebeck coefficient in the EDLT of large-area graphene on the flexible substrate as a function of $V_G - V_{\text{CNP}}$. **d** The power factor ($S^2\sigma$) in the EDLT of large-area graphene on the flexible substrate as a function of $V_G - V_{\text{CNP}}$.

of S in the EDLT composed of large-area graphene on a flexible substrate. As shown in Fig. 2c, we achieved continuous control of S in the graphene-based EDLT on the PET substrate, and the shift in the polarity in S was reasonably observed. Interestingly, we observed the maximum S value in the hole-doping ($57.1 \mu\text{V K}^{-1}$) and electron-doping ($-36.6 \mu\text{V K}^{-1}$) regions. Notably, the difference in the maximum S between hole and electron doping has been previously reported, and this is most likely due to the effect of charged impurities on the substrates.^{12–14} Importantly, the $S - \sigma$ relationship indicated no hysteresis behavior, meaning that we succeeded in the measurement of intrinsic thermoelectric properties in these CVD-grown large-area graphene films (see Supplementary Information S2). Because the gate voltage dependences of the electrical conductivity (σ) and the Seebeck coefficient (S) were collected, we evaluated the gate voltage dependence of the power factor ($S^2\sigma$). As shown in Fig. 2d, similar to the results of S , we obtained the peak power factor in the hole-doping ($6.93 \pm 0.29 \text{ mW m}^{-1} \text{ K}^{-2}$) and electron-doping ($3.29 \pm 0.10 \text{ mW m}^{-1} \text{ K}^{-2}$) regions.

DISCUSSION

To demonstrate the performance of our samples, in Tables 1 and 2, we summarize the previous reports on flexible large-scale van der Waals materials, organic conducting polymers, CVD-grown polycrystalline graphene films, and single-crystal graphene films.^{3–14,26–28} As shown in Fig. 3a, b, the peak power factors of our samples are higher than the best previously reported values among flexible large-scale van der Waals materials.^{7,11} Therefore, we can conclude that the CVD-grown large-area polycrystalline graphene film is a strong candidate for the power generator of IoT devices.

Table 1. Comparison of the maximum hole power factors ($S^2\sigma$) of van der Waals materials. The results of the electrical conductivity (σ) and the Seebeck coefficient (S) at the maximum $S^2\sigma$ are also listed

Hole	σ (S/cm)	S ($\mu\text{V/K}$)	$S^2\sigma$ (mW/(m K ²))
This work	28900	49	6.93
PEDOT:PSS [Ref. 3]	880	73	0.469
PEDOT:Tos [Ref. 4]	1770	54	0.505
As-grown FLG [Ref. 24]	28241	11.44	0.37
TPA-attached CVD-grown FLG [Ref. 25]	1063	41	0.18
O ₂ -plasma treated CVD-grown FLG [Ref. 26]	320	41	0.055
CNT yarn [Ref. 7]	7476	57	2.39
SWNT films [Ref. 8]	3210	87.96	2.48
Carbon-based polymer nanocomposite [Ref. 11]	1900	120	2.71
SC SLG on hBN [Ref. 12]	~11700	176	~36.0
SC SLG on SiO ₂ [Ref. 13]	~15400	65.7	~6.60
SC DLG on SiO ₂ [Ref. 14]	~7900	77.8	~4.80

We also compare our results with other CVD-grown polycrystalline graphene films.^{26–28} Although there has been no report on the thermoelectric properties of millimeter-scale polycrystalline graphene films prior to this study, the power factors of several hundred micron-scale graphene films have already been investigated. However, it should be noted that these previous studies did

not perform thermoelectric measurements using the transistor configuration. Therefore, the carrier densities of previous studies are not optimized, and a fair comparison of maximum power factors among the other polycrystalline graphene samples is impossible. Interestingly, as summarized in Table 1 and Fig. 3a, our result is approximately one order of magnitude larger than that of previous reports. This difference might be understood by the optimized carrier doping in our samples. As shown in Fig. 3, we

Electron	σ (S/cm)	S ($\mu\text{V/K}$)	$S^2\sigma$ (mW/(m $\cdot\text{K}^2$))
This work	31000	-32.6	3.29
PEDOT:PSS mixed with n-Bi ₂ Te ₃ particles [Ref. 5]	56	-120	0.081
Poly[K _x (Ni-ett)] [Ref. 6]	45	-121.6	0.066
CNT yarn [Ref. 7]	7850	-56	2.46
PEI-doped CNT [Ref. 9]	3630	-64	1.49
NaBH ₄ -doped CNTs [Ref. 10]	52	-86	0.038
SC SLG on hBN [Ref. 12]	~9600	-140	~19.0
SC SLG on SiO ₂ [Ref. 13]	~28100	-46.9	~6.18
SC DLG on SiO ₂ [Ref. 14]	~9600	-65.2	~4.10

have succeeded in tuning the thermoelectric properties of CVD-grown polycrystalline graphene films via an EDLT.

Because there are several reports on optimized carrier doping in single-crystal graphene films, we also compare our results with reports on single crystals to understand the reason for the high performance of our samples.^{12–14} As shown in Tables 1 and 2, the Seebeck coefficient values at the maximum power factors in our polycrystalline films are slightly lower than those of single-crystal graphene samples. In contrast, very surprisingly, we obtained single-crystal-like high electrical conductivity at the maximum power factors in our samples. Consequently, the maximum power factors in our CVD-grown polycrystalline graphene were close to the values in single-crystal graphene. According to the above arguments, interestingly, we suggest that S and σ are not seriously affected by the grain-boundary effect in our samples. Therefore, the extremely high electrical conductivity in our films is expected to be an important point for understanding their high power factors.

To clarify the mechanism of the high electrical conductivity, we measured the temperature dependences of the electrical conductivity in the graphene-based EDLT sample. Figure 4a shows the temperature dependences of the four-point-probe electrical conductivity at gate voltages of -1.5, 0.3, and 1.5 V. The temperature range is set below 220 K, which is lower than the freezing temperature of the ionic gel film. As shown in Fig. 4a, when the gate voltage was close to V_{CNP} ($V_{\text{G}} = 0.3$ V), the electrical conductivity decreased with decreasing temperature. This insulating behavior suggests that the transport property near the CNP is

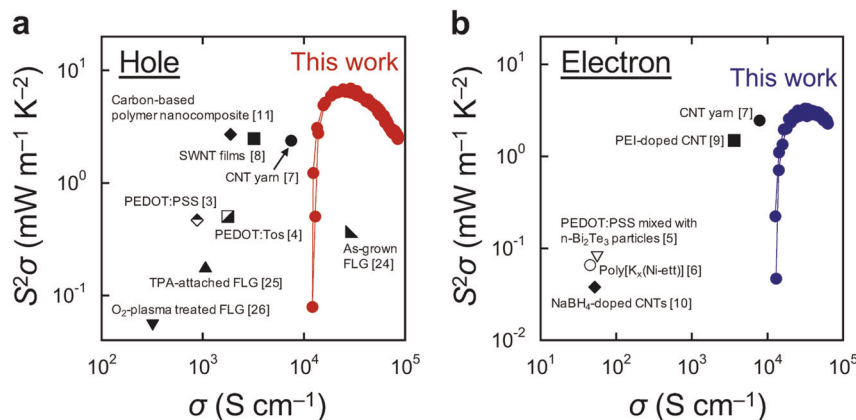


Fig. 3 Summary of the power factors ($S^2\sigma$) in van der Waals materials. Comparison of the **a** holes and **b** electrons in flexible large-scale van der Waals materials

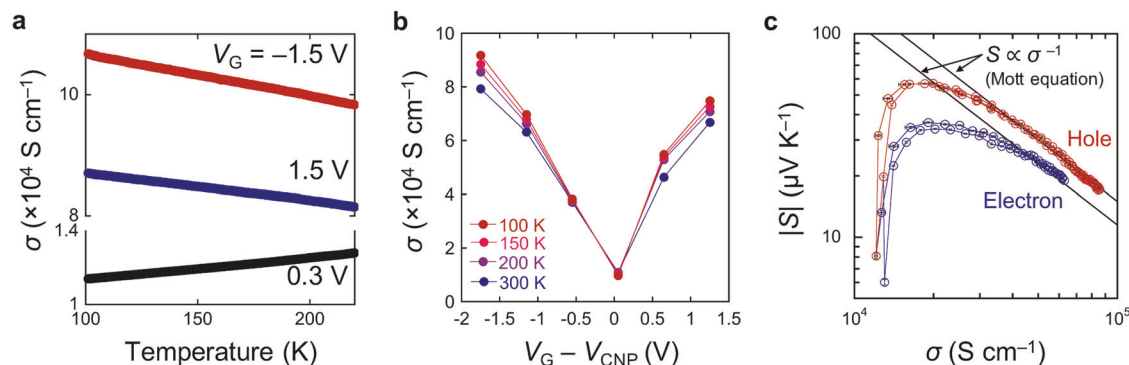


Fig. 4 **a** The temperature dependences of electrical conductivity at gate voltages of -1.5, 0.3, and 1.5 V. The temperature range is set below 220 K, which is lower than the freezing temperature of the ionic gel film. **b** The electrical conductivities at various temperatures as a function of $V_{\text{G}} - V_{\text{CNP}}$. **c** The $|S| - \sigma$ relationships in hole and electron carriers. The trend of $S \propto \sigma^{-1}$, which is explained by the Mott equation, is also indicated

possibly determined by the trap and/or mid-gap states induced by the polycrystalline nature of our films. On the other hand, as shown in Fig. 4a, metallic behavior was observed in both the p- ($V_G = -1.5$ V) and n-doping ($V_G = 1.5$ V) regions, indicating that the charge transport mechanism changed from insulating to metallic by carrier doping. To gain more details about the change in the transport property, Fig. 4b summarizes the electrical conductivities at various temperatures as a function of $V_G - V_{CNP}$. Except for the result of $V_G - V_{CNP} \sim 0$ V, the electrical conductivity increased with decreasing temperature at all gate voltages. Furthermore, as shown in Fig. 4c, the $S - \sigma$ relationships for both the hole and electron carriers follow the trend of $S \propto \sigma^{-1}$ in the high conductivity region. This $S \propto \sigma^{-1}$ relationship is explained by the Mott equation, which describes the thermoelectric properties in metallic states (see Supplementary Information S3).²⁹ Therefore, we can conclude that the excellent electrical conductivity and high thermoelectric performances in CVD-grown large-area graphene films on the PET substrate originate from the filling of trap states by the EDLT technique.

Finally, we should comment on future challenges to realize flexible thermoelectric batteries based on two-dimensional (2D) materials. In general, the conversion efficiency of thermoelectric materials is evaluated by the dimensionless figure of merit, $zT = S^2\sigma T/\kappa$, where T and κ are the temperature and the thermal conductivity, respectively. Based on our experimental results and previous work,³⁰ the zT of our films is estimated to be 0.003 at 300 K. On the other hand, 2D TMDCs are expected to be promising materials because of their high Seebeck coefficient and low thermal conductivity.^{31–33} By combining the experimental and theoretical values, a zT value of 0.5 is predicted in TMDC materials.³¹ However, we would like to suggest that these trends are not simply applicable to 2D materials. Since the atomically thin thermoelectric materials are prepared on thicker thermally insulating flexible substrates, the induced temperature difference is mainly determined by the substrate. Although the thermal conductivity of graphene is extremely high, in this work, a large ΔT was induced in the graphene films by the PET substrate. Therefore, we can expect that the power factor of the active materials and the thermal transport properties including the substrate are more crucial for future 2D thermoelectric generators.

Furthermore, we calculated the output power of flexible thermoelectric generators based on the optimized graphene films (see Supplementary Information S4). Under the simplified conditions of no contact resistance, a temperature difference of 5 K, and an active area of 50–100 cm², the maximum output power reaches ~ 1 –10 μ W, which is enough to operate wearable IoT devices, sensors, and processors. We should also compare our results with other energy harvesting technologies, such as photovoltaic, piezoelectric, and triboelectric techniques. Although these technologies can generate power greater than 10 μ W, it is very difficult for them to operate continuously for a long time. For instance, photovoltaic batteries cannot generate electric power at night and on rainy days, and piezoelectric and triboelectric batteries require frequent mechanical motion for power generation. Therefore, thermoelectric energy harvesting is more suitable for wearable IoT devices.

In summary, we investigated the thermoelectric properties of CVD-grown large-area graphene films on a PET substrate by electric double layer gating. We achieved ambipolar transfer characteristics and realized the continuous modulation of positive and negative Seebeck coefficients. Moreover, the power factors in both the hole- and electron-doped regions indicated a dome-like structure by tuning the Fermi level of the polycrystalline large-area graphene films. Finally, their maximum power factors exceed the best recorded values among flexible large-scale van der Waals materials. These results strongly suggest that the CVD-grown large-area polycrystalline graphene film is a promising candidate for thermoelectric power generators.

METHODS

Sample preparation

Polycrystalline Cu foil samples (23 cm \times 20 cm \times 33 μ m thick) were treated with Ar/H₂ plasma at 5 Pa for 20 min to clean their surfaces before the CVD process. After cleaning, CVD was performed (CVD conditions: 3 Pa, CH₄/Ar/H₂ = 30/20/10 standard cubic centimeters per minute, 4.5 kW for each microwave generator). The synthesized graphene films were transferred onto a PET substrate (188 μ m thick). The device fabrication process was as follows. First, we cut the original CVD-grown large-area graphene film on the PET substrate into smaller pieces (1 cm \times 1 cm) and patterned them by oxygen plasma treatment for 300 s using adhesive tape as a shadow mask. Second, Au/Ni (30 nm/5 nm) electrodes were thermally deposited onto the graphene samples. Finally, for the gate dielectric, we selected an ion gel, which is a mixture of an ionic liquid ([DEME][TFSI]) and organic polymer (P(VDF-HFP)). The gate dielectric layer was prepared by drop-casting onto the graphene samples.

Experimental details of the measurements of thermoelectric properties

The transfer characteristics of the graphene EDLT samples were evaluated using a semiconductor parameter analyzer (Agilent, B1505A) in an N₂-filled glove box at room temperature. We applied a constant drain voltage of -0.1 V and gate voltages ranging from 1.5 V to -1.5 V. The four-point-probe electrical conductivity was estimated from the current-voltage curves by applying a drain voltage from -0.1 to 0.1 V. The voltage drop between the two voltage probes in the four-point-probe configuration was monitored using a nanovoltmeter (Keysight 34420A). Along with the measurements of the transistor characteristics, thermoelectric measurements were performed. The EDLT sample was fixed on two Peltier elements (Laird Technologies CP1.0-31-05L), which were wired in series with a DC power supply (Keysight B2902A). To measure the temperature difference between the source and drain electrodes, we placed two K-type (alumel–chromel) thermocouples (Sakaguchi EH VOC Corp. TCKT0051) on the surface of the sample. The measured temperature was monitored by a temperature controller (Lakeshore model 335). In the measurement of the Seebeck coefficient, we turned on two Peltier elements to cause a temperature difference, and the generated thermoelectromotive force was simultaneously measured using a nanovoltmeter (Keysight 34420A).

Measurements of charge transport properties using the graphene EDLT on the PET substrate

Low-temperature experiments were performed in a physical property measurement system (PPMS, Quantum Design, model 6000). The gate voltage was applied at 300 K by applying the -10 mV drain voltage. The transistor characteristics were monitored by a semiconductor parameter analyzer (Agilent Technologies, Inc. B1500A). Simultaneously, the voltage drop between the two voltage probes in the four-point-probe configuration was measured using a nanovoltmeter (Hewlett-Packard 34420A). We monitored the drain current in the temperature range from 300 to 100 K at each gate voltage.

DATA AVAILABILITY

All data related to the manuscript are available on request from the corresponding author.

Received: 8 July 2019; Accepted: 22 October 2019;
Published online: 08 November 2019

REFERENCES

1. Bahk, J.-H., Fang, H., Yazawa, K. & Shakouri, A. Flexible thermoelectric materials and device optimization for wearable energy harvesting. *J. Mater. Chem. C* **3**, 10362–10374 (2015).
2. Kim, S. J. et al. High-performance flexible thermoelectric power generator using laser multiscanning lift-off process. *ACS Nano* **20**, 10851–10857 (2016).
3. Kim, G.-H., Shao, L., Zhang, K. & Pipe, K. P. Engineered doping of organic semiconductors for enhanced thermoelectric efficiency. *Nat. Mater.* **12**, 719–723 (2013).
4. Bubnova, O. et al. Semi-metallic polymers. *Nat. Mater.* **13**, 190–194 (2014).

5. Zhang, B., Sun, J., Kats, H. E., Fang, F. & Opila, R. L. Promising thermoelectric properties of commercial PEDOT:PSS materials and their Bi₂Te₃ powder composites. *ACS Appl. Mater. Interfaces* **2**, 3170–3178 (2010).
6. Sun, Y. et al. Organic thermoelectric materials and devices based on p- and n-Type Poly(metal 1,1,2,2-ethenetetrathiolate)s. *Adv. Mater.* **24**, 932–937 (2012).
7. Choi, J. et al. Flexible and robust thermoelectric generators based on all-carbon nanotube yarn without metal electrodes. *ACS Nano* **11**, 7608–7614 (2017).
8. Zhou, W. et al. Ultrahigh-power-factor carbon nanotubes and an ingenious strategy for thermoelectric performance evaluation. *Small* **12**, 3407–3414 (2016).
9. Zhou, W. et al. High-performance and compact-designed flexible thermoelectric modules enabled by a reticulate carbon nanotube architecture. *Nat. Commun.* **8**, 14486 (2017).
10. Kim, S. L., Choi, K., Tazebay, A. & Yu, C. Flexible power fabrics made of carbon nanotubes for harvesting thermoelectricity. *ACS Nano* **8**, 2377–2386 (2017).
11. Cho, C. et al. Outstanding low temperature thermoelectric power factor from completely organic thin films enabled by multidimensional conjugated nano-materials. *Adv. Energy Mater.* **6**, 1502168 (2016).
12. Duan, J. et al. High thermoelectric power factor in graphene/hBN devices. *Proc. Natl Acad. Sci. USA* **113**, 14272–14276 (2016).
13. Zuev, Y. M., Chang, W. & Kim, P. Thermoelectric and magnetothermoelectric transport measurements of graphene. *Phys. Rev. Lett.* **102**, 96807 (2009).
14. Nam, S.-G., Ki, D.-K. & Lee, H.-J. Thermoelectric transport of massive Dirac fermions in bilayer graphene. *Phys. Rev. B* **82**, 245416 (2010).
15. Bae, S. et al. Roll-to-roll production of 30-inch graphene films for transparent electrodes. *Nat. Nanotechnol.* **5**, 574–578 (2010).
16. Kim, J. et al. Low-temperature synthesis of large-area graphene-based transparent conductive films using surface wave plasma chemical vapor deposition. *Appl. Phys. Lett.* **98**, 91502 (2011).
17. Ye, J. et al. Accessing the transport properties of graphene and its multilayers at high carrier density. *Proc. Natl Acad. Sci. USA* **108**, 13002–13006 (2011).
18. Chien, Y.-Y., Yuan, H., Wang, C.-R. & Lee, W.-L. Thermoelectric power in bilayer graphene device with ionic liquid gating. *Sci. Rep.* **6**, 20402 (2016).
19. Kanahashi, K. et al. Formation of environmentally stable hole-doped graphene films with instantaneous and high-density carrier doping via a boron-based oxidant. *npj 2D Mater. Appl.* **3**, 7 (2019).
20. Yamada, T., Ishihara, M. & Hasegawa, M. Large area coating of graphene at low temperature using a roll-to-roll microwave plasma chemical vapor deposition. *Thin Solid Films* **532**, 89–93 (2013).
21. Yamada, T., Ishihara, M., Kim, J., Hasegawa, M. & Iijima, S. A roll-to-roll microwave plasma chemical vapor deposition process for the production of 294 mm width graphene films at low temperature. *Carbon* **50**, 2615–2619 (2012).
22. Pu, J. et al. Enhanced thermoelectric power in two-dimensional transition metal dichalcogenide monolayers. *Phys. Rev. B* **94**, 14312 (2016).
23. Ohta, H. et al. Unusually large enhancement of thermopower in an electric field induced two-dimensional electron gas. *Adv. Mater.* **24**, 740–744 (2012).
24. Yanagi, K. et al. Tuning of the thermoelectric properties of one-dimensional materials networks by electric double layer techniques using ionic liquids. *Nano Lett.* **14**, 6437–6442 (2014).
25. Shimizu, S. et al. Thermoelectric detection of multi-subband density of states in semiconducting and metallic single-walled carbon nanotubes. *Small* **12**, 3388 (2016).
26. Babichev, A. V., Gasumyants, V. E. & Butko, V. Y. Resistivity and thermopower of graphene made by chemical vapor deposition technique. *J. Appl. Phys.* **113**, 076101 (2013).
27. Sim, D. et al. Power factor enhancement for few-layered graphene films by molecular attachments. *J. Phys. Chem. C* **115**, 1780–1785 (2011).
28. Xiao, N. et al. Enhanced thermopower of graphene films with oxygen plasma treatment. *ACS Nano* **5**, 2749–2755 (2011).
29. Mott, N. F. & Davis, E. Electronic Processes of Non-Crystalline Material (Clarendon, 1979).
30. Lee, W. et al. In-plane thermal conductivity of polycrystalline chemical vapor deposition graphene with controlled grain sizes. *Nano Lett.* **17**, 2361–2366 (2017).
31. Zhang, G. & Zhang, Y.-W. Thermoelectric properties of two-dimensional transition metal dichalcogenides. *J. Mater. Chem. C* **5**, 7684–7698 (2017).
32. Hippalgaonkar, K. et al. High thermoelectric power factor in two-dimensional crystals of MoS₂. *Phys. Rev. B* **95**, 115407 (2017).
33. Cai, Y., Lan, J., Zhang, G. & Zhang, Y.-W. Lattice vibrational modes and phonon thermal conductivity of monolayer MoS₂. *Phys. Rev. B* **89**, 035438 (2014).

ACKNOWLEDGEMENTS

We thank H. Horii, T. Yamamoto, and H. Fukuyama for valuable discussions. K.K. acknowledges the Leading Graduate Program in Science and Engineering, Waseda University, from the Ministry of Education, Culture, Sports, Science and Technology in Japan (MEXT). T.T. is partially supported by JSPS KAKENHI (Grant Numbers JP26102012, JP25000003, 19K22127, and JP17H01069) and JST CREST (Grant Number JPMJCR1715). H.O. is supported by JSPS KAKENHI (JP17H01314, 19H05791) and the Asahi Glass Foundation. This work was performed under the Research Program for Next Generation Young Scientists of "Network Joint Research Center for Materials and Devices: Dynamic Alliance for Open Innovation Bridging Human, Environment and Materials."

AUTHOR CONTRIBUTIONS

T.T. conceived the project and designed the experiments. K.K. performed all measurements and carried out the data analysis. M.I. and M.H. performed the surface wave plasma CVD of large-area graphene films. H.O. assisted in the preparation of the thermopower measurement system. All the authors interpreted the data, commented on the manuscript, and agreed with the results and conclusions.

COMPETING INTERESTS

The authors declare no competing interests.

ADDITIONAL INFORMATION

Supplementary information is available for this paper at <https://doi.org/10.1038/s41699-019-0128-0>.

Correspondence and requests for materials should be addressed to T.T.

Reprints and permission information is available at <http://www.nature.com/reprints>

Publisher's note Springer Nature remains neutral with regard to jurisdictional claims in published maps and institutional affiliations.



Open Access This article is licensed under a Creative Commons Attribution 4.0 International License, which permits use, sharing, adaptation, distribution and reproduction in any medium or format, as long as you give appropriate credit to the original author(s) and the source, provide a link to the Creative Commons license, and indicate if changes were made. The images or other third party material in this article are included in the article's Creative Commons license, unless indicated otherwise in a credit line to the material. If material is not included in the article's Creative Commons license and your intended use is not permitted by statutory regulation or exceeds the permitted use, you will need to obtain permission directly from the copyright holder. To view a copy of this license, visit <http://creativecommons.org/licenses/by/4.0/>.

© The Author(s) 2019